SAGE-Hindawi Access to Research
International Journal of Electrochemistry
Volume 2011, Article ID 249804, 13 pages
doi:10.4061/2011/249804

Research Article

Carbon-Supported Fe Catalysts for CO_2 Electroreduction to High-Added Value Products: A DEMS Study: Effect of the Functionalization of the Support

S. Pérez-Rodríguez,[1] G. García,[2,3] L. Calvillo,[1] V. Celorrio,[1] E. Pastor,[2] and M. J. Lázaro[1]

[1] *Instituto de Carboquímica CSIC, Miguel Luesma Castán 4, 50018 Zaragoza, Spain*
[2] *Departmento de Química-Física, Instituto Universitario de Materiales y Nanotecnología, Universidad de La Laguna, Avenida Astrofísico F. Sánchez s/n, 38071 La Laguna, Spain*
[3] *Instituto de Catálisis y Petroleoquímica, CSIC, c/Marie Curie 2, 2. 28049 Madrid, Spain*

Correspondence should be addressed to G. García, gonzalo@icp.csic.es and M. J. Lázaro, mlazaro@carbon.icb.csic.es

Received 30 April 2011; Accepted 9 September 2011

Academic Editor: Maria E. Martins

Vulcan XC-72R-supported Fe catalysts have been synthesised for the electroreduction of CO_2 to high-added value products. Catalysts were obtained by the polyol method, using ethylene glycol as solvent and reducing agent. Prior to the metal deposition, Vulcan was subjected to different oxidation treatments in order to modify its surface chemistry and study its influence on the physicochemical and electrochemical properties of the catalysts, as well as on the product distribution. The oxidation treatments of the supports modify their textural properties, but do not affect significantly the physicochemical properties of catalysts. However, DEMS studies showed that the carbon support degradation, the distribution of products, and the catalytic activity toward the CO_2 electroreduction reaction depend significantly on the surface chemistry of the carbon support.

1. Introduction

Carbon dioxide (CO_2) emissions are the inevitable result from the burning of fossil fuels for electricity and energy (80% anthropogenic CO_2) [1]. During the last years, CO_2 concentration in the atmosphere has been increasing, being the major responsible of global warming. Therefore, reducing the CO_2 concentration in the atmosphere has become a critical issue. Different methods have been developed to reduce its emissions, such as chemical, thermochemical, photochemical, electrochemical, and biochemical procedures [2–4]. Among them, the electrochemical reduction seems to be of particular interest since it could both mitigate the greenhouse gas emission and use CO_2 as carbon source for producing a variety of useful products like (e.g., formic acid, methanol, etc.) for energy source [1, 4–8]. CO_2 reduction would be carried out making use of renewable energy to result in a net decrease of CO_2 emissions [9, 10].

In recent years, different metallic electrodes have been studied for the electrochemical reduction of carbon dioxide, since the product distribution strongly depends on the used material, surface metallic arrangement, and surface energy [11–17]. Copper has been found to be one of the most effective electrode materials for the CO_2 reduction process at atmospheric pressure and room temperature in aqueous solutions [11, 12, 16]. On the other hand, CO_2 is hardly reduced on group VIII-X metal electrodes such as Fe, Co, and Ni, under similar conditions [15–17].

One of the main problems of this process is the low solubility of CO_2 in water at atmospheric pressure and room temperature. For this reason, in the last years, the electroreduction of CO_2 has been studied at high pressure [18–21] or low temperatures [21–24] on different metal electrodes. It has been reported that, at low temperatures (ca. 2°C) or high pressures (ca. 30 atm), the catalytic activity of the electrodes toward the electrochemical CO_2 reduction increases and the selectivity of the resultant products can change, even for metal catalysts of the group VIII-X [18–24]. In this context, Azuma et al. reported that the CO_2

reduction efficiency increased dramatically on some metal electrodes, such as Ni, as the temperature decreased [24]. Conversely, at high pressure, formic acid and/or carbon monoxide are efficiently formed on metal electrodes of the group VIII-X. Moreover, the formation of short and long chain hydrocarbons such as methane, ethane, propane, and iso- and normal-butanes has also been observed on Fe, Co, and Ni electrodes [18–20].

Since the solubility of CO_2 in aprotic solvents is higher than in water, the electroreduction of CO_2 has also been studied using organic molecules (methanol, acetonitrile, dimethyl formamide, propylene carbonate, etc.) as reaction medium [25–32]. Higher CO_2 solubility increases the current density, however, the low electrolytic conductivity gives high ohmic losses. For this reason, methanol is often added into a supporting electrolyte in order to balance these two aspects. For example, Kaneco et al. reported that the faradic efficiencies for CO_2 reduction products using Cu electrode in a methanol solution at low temperatures were better than those obtained without methanol at ambient temperature [29, 30]. In addition, Ohta et al. reported the formation mainly of methane, carbon monoxide and ethane, on different metal electrodes (among them Fe, Co, and Ni) using methanol into the supporting electrolyte [27].

Therefore, the effective electrochemical reduction of CO_2 on metal surfaces of the group VIII-X using high pressures, low temperatures, and/or nonaqueous solvents has been demonstrated. Among these metals, Fe is well known as catalyst for the hydrocarbon formation in the Fischer-Tropsch reaction. Therefore, its catalytic activity toward the electrochemical CO_2 reduction is expected to be interesting [33].

On the other hand, carbon materials have also been used as electrodes for the electrochemical CO_2 reduction. However, until now, the electrocatalytic activity of these electrodes is not clear. Christensen et al. reported that CO_2 is reduced to CO and carbonate on a glassy carbon electrode in acetonitrile solution [32]. Moreover, Hara et al. reported the formation of hydrocarbons such as methane, ethane, ethylene, propane, and n-butane during the electrochemical CO_2 reduction on a glassy carbon electrode under 30 atm [34]. However, there are not many studies about the electroreduction of CO_2 on metal catalysts supported on carbon materials in aqueous electrolytes. These electrodes could have different properties than those of the corresponding metal or carbon material. The support could improve the dispersion of the metal and, therefore, the activity and/or selectivity could be changed. Nowadays, among all kinds of carbon supports, carbon blacks are the most commonly used, especially for electrochemical applications (e.g., in the fuel cells field), due to their mesoporous distribution and their graphite characteristics. Vulcan XC-72 is the most frequently used because of its good compromise between electrical conductivity and high specific surface area [35, 36]. The surface chemistry of carbon materials can be modified by oxidation treatments in gas or liquid phase in order to create functional groups. These functional groups may significantly affect the dispersion and anchoring of the metal on the carbon materials and, therefore, may affect the performance of the electrocatalysts. In addition, it is well known that surface oxygen groups are the responsible for both the acid-base and the redox properties of the carbon materials. It has been reported that the acidic groups on the carbon surface decrease the hydrophobicity of the carbon, whereas the less acidic groups improve the interaction between metal particles and carbon materials [37]. However, the functionalization of Vulcan XC-72R has not been studied for the CO_2 electroreduction reaction.

Table 1: Nomenclature of functionalizated Vulcan XC-72R.

Sample	Oxidizing agent	Temperature (°C)	Time (h)
Vulcan	—	—	—
Vulcan NSTa0.5	HNO_3-H_2SO_4 1 : 1 (v/v)	25	0.5
Vulcan NcTb0.5	Concentrated HNO_3 (65%)	115	0.5
Vulcan NcTb2	Concentrated HNO_3 (65%)	115	2

In this work, different Fe catalysts supported on Vulcan XC-72R have been prepared for studying the electroreduction of CO_2 in aqueous solution under 1 atm and room temperature. Prior to the metal deposition, Vulcan was subjected to different oxidation treatments, using HNO_3 or HNO_3-H_2SO_4 1 : 1 (v/v) mixture as oxidizing agents, in order to create functional groups. In this way, the influence of the surface chemistry of the carbon support on the physicochemical and electrochemical properties of the catalysts for the CO_2 electroreduction process can be studied.

In the present communication, the modified and unmodified carbon supports were characterized by X-ray diffraction (XRD), scanning electron microscopy (SEM), temperature programmed desorption (TPD), and N_2-physisorption. On the other hand, carbon-supported catalysts (Fe/C) were characterized by energy dispersive X-ray analysis (EDX), XRD, SEM, and N_2-physisorption. In addition, the electrochemical properties of the catalysts and the formation of gaseous and volatile products of the reduction of CO_2 were followed by *in-situ* differential electrochemical mass spectrometry (DEMS).

2. Experimental

2.1. Functionalization of Vulcan XC-72R. In order to create functional groups, Vulcan XC-72R (Cabot) was modified with different oxidation treatments in liquid phase, using concentrated HNO_3 (65% wt.) (Nc) and an HNO_3-H_2SO_4 1 : 1 (v/v) mixture (NS) as oxidizing agents [38]. The oxidation treatments were carried out at room (T_a) and boiling temperature (T_b) for 0.5 or 2 h. The nomenclature used for the different materials and the oxidation conditions are summarized in Table 1.

2.2. Synthesis of the Carbon-Supported Fe Electrocatalysts. Fe electrocatalysts were prepared by polyol method, using ethylene glycol (EG) as solvent and reducing agent. The

synthesis involved the following steps: first, the metal precursor, $Cl_3Fe \cdot 6H_2O$ (Sigma-Aldrich), was dissolved in ethylene glycol under sonication and the pH was adjusted to 11 using a 1 M NaOH/EG solution. Then, a known amount of Vulcan was added to the metal solution and the resultant suspension was heated at 195°C for 2 h under mechanical stirring. Subsequently, the mixture was quickly cooled in a cold-water bath and the pH was adjusted to 1 using HCl (37%, Sigma-Aldrich). Finally, catalysts were filtered, washed with water, and dried at 70°C. Appropriate amounts of metal precursors were used to obtain a theoretical metal loading of 20 wt.%.

2.3. Physicochemical Characterization. Metal content of the electrocatalysts was obtained using a Hitachi S-3400 N microscope coupled to a Röntec XFlash analyzer.

Temperature programmed desorption (TPD) experiments were carried out in a U-shaped quartz reactor using a Micromeritics Pulse Chemisorb 2700. The temperature was increased positively at a rate of 10°C min^{-1} up to 1050°C under Ar flow. The amounts of CO and CO_2 desorbed from the carbon samples were analyzed online by mass spectroscopy using a Thermostar GSD 301 T (Balzers).

Nitrogen adsorption and desorption isotherms were measured at −196°C using a Micromeritics ASAP 2020. The total surface area was determined using the (Brunauer, Emmett and Teller) BET equation and total pore volume was determined using the single point method at $P/P_0 = 0.99$. The micropore volume was determined using the t-plot method. Pore size distribution (PSD) curves were obtained from the analysis of the adsorption branch of the nitrogen isotherm using the (Barrett, Joyner and Halenda) BJH method. The maximum of the PSD was used as the average pore diameter.

X-Ray diffraction (XRD) patterns were recorded using a Bruker AXS B8 Advance diffractometer with a θ-θ configuration and using Cu Kα radiation.

2.4. Preparation of Working Electrodes. The working electrodes (7 mm of diameter, 0.25 mm of thickness) were prepared depositing a layer of the catalysts ink onto one side of a carbon cloth previously treated at 320°C for 1 h. Catalyst inks were prepared by mixing 0.5 mg of catalyst, 0.01 g of Nafion dispersion (5 wt.%, Sigma-Aldrich), and 10 μL of ultrapure water. The final metal load of the working electrodes was 0.26 mg Fe/cm^2.

2.5. DEMS Setup. A scheme of the DEMS setup used for the in situ spectrometric and electrochemical measurements is described in detail in [39]. Briefly, the working electrode (WE) is fixed between a PTFE membrane (Scimat) and a carbon glassy rod, which also keeps the electric contact. The cell was designed to follow "in-situ" the electrochemical properties of electrodes and, simultaneously, the gaseous species produced on the electroactive surface through mass spectrometry. Thus, the experimental setup allows the simultaneous acquisition of mass spectrometric cyclic voltammograms (MSCVs) for selected *m/z* (mass to charge) ratios and conventional voltammograms (CVs) or simultaneous mass spectrometric transients (MSTs) and conventional current transient curves.

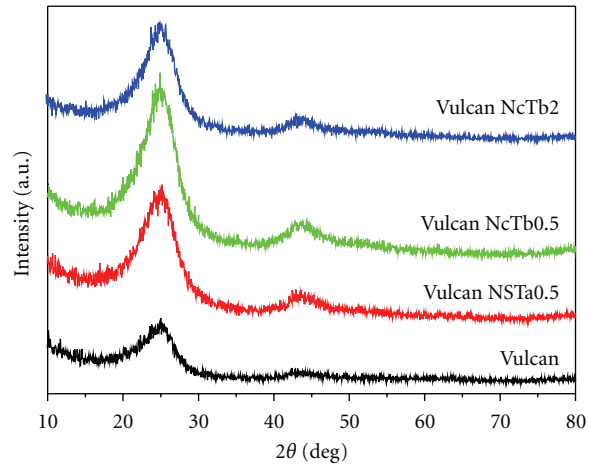

Figure 1: XRD patterns of carbon supports.

2.6. Electrochemical Measurements. Electrochemical experiments were carried out in a three-electrode electrochemical cell at room temperature and atmospheric pressure. A large area carbon rod was used as a counter electrode, whereas an Ag/AgCl/Sat. KCl electrode placed inside a Luggin capillary was employed as reference. All potentials in the text are referred to this electrode. The potenciostat-galvanostat was an Autolab PGSTAT302 (Ecochemie). The electrochemical cell was directly attached to the vacuum chamber of a mass spectrometer (Balzers QMG112) with a Faraday cup detector.

The working electrode was immersed into 0.5 M H_2SO_4 (Merck, p.a.) electrolyte solution, which was deaerated with argon (N50). In order to analyze the activity of catalysts towards the reduction of CO_2, previously to each measure, CO_2 (99,99%, Air Liquide) was bubbled during 30 min.

3. Results

3.1. Characterization of the Supports. SEM and XRD techniques were used to study the morphology of carbon support, before and after the oxidation treatments. SEM images (not shown) prove that Vulcan XC-72R is formed by an aggregation of spherical carbon nanoparticles (primary particles) with range sizes of 30–60 nm. After the oxidation treatments, the structure of Vulcan was not altered significantly. However, the most severe oxidation treatment (NcTb2) resulted in a partial destruction of its morphology, since primary particles did not show a spherical shape.

Figure 1 shows the XRD patterns of all the carbon supports. In all the samples, a peak around $2\theta = 25°$ was observed, which is associated to the graphite (002) diffraction line. Also, (100) and (101) reflections of the graphite, at $2\theta = 24.8°$ and $2\theta = 43.5°$, can be observed. These peaks confirm that Vulcan has an intermediate structure between

Table 2: Quantification of surface oxygen groups as CO and CO_2 amounts desorbed during the TPD experiments.

Sample	CO_2 and CO peak area (μmolg^{-1})					$CO + CO_2$ (μmolg^{-1})	CO/CO_2
	Carboxylic	Lactone	Anhydride	Phenol	Quinone + carbonyl		
Vulcan	—	—	—	—	—	—	—
Vulcan NSTa0.5	545	256	65	412	881	2160	1.54
Vulcan NcTb0.5	556	243	58	480	699	2037	1.42
Vulcan NcTb2	799	362	63	632	963	2819	1.34

Table 3: Textural properties of the supports and Fe electrocatalysts.

Sample	S_{BET} (m^2/g)	S_{MICRO} (m^2/g)	S_{MESO} (m^2/g)	V_{TOTAL} (cm^3/g)	V_{MICRO} (cm^3/g)	V_{MESO} (cm^3/g)
Vulcan	210	102	108	0.38	0.06	0.32
Vulcan NSTa0.5	200	104	96	0.40	0.06	0.34
Vulcan NcTb0.5	181	91	90	0.38	0.05	0.33
Vulcan NcTb2	159	77	82	0.38	0.04	0.33
Fe/Vulcan	175	76	99	0.41	0.04	0.36
Fe/Vulcan NSTa0.5	166	55	111	0.49	0.03	0.46
Fe/Vulcan NcTb0.5	148	58	90	0.41	0.03	0.37
Fe/Vulcan NcTb2	139	54	85	0.42	0.03	0.38

amorphous and graphitic. After the oxidation treatments, the same peaks were observed, indicating that the original structure of Vulcan was maintained. However, the intensity of the peaks increased with the severity of the oxidation treatment, except for the sample Vulcan NcTb2. This increase is attributed to the removal of the more amorphous carbon. In other words, the structure ratio crystalline/amorphous increases. On the other hand, the sample Vulcan NcTb2 did not follow the same tendency, which is attributed to the partial destruction of the original structure of Vulcan (i.e., both amorphous and crystalline structures are damaged), as observed by SEM.

The surface chemistry of the supports was studied by TPD experiments. These measurements give information about the surface oxygen groups created during the oxidation treatments. Acidic groups (carboxylic groups, lactones, and anhydrides) are decomposed into CO_2 at lower temperatures and basic and neutral groups (anhydrides, phenols, quinones and carbonyls) are decomposed into CO at higher temperatures during the TPD experiments [40]. In order to estimate the type and the amount of oxygen groups created during the oxidation treatments, CO_2 and CO profiles can be deconvoluted. Thus, the decomposition temperature can be related to the type of the functional groups created [40]. Deconvolution profiles were carried out with Excel software, using a Gaussian function to fit each functional group contribution and the corresponding addition of Gaussian curves was fitted minimizing the square of the deviations by a numerical routine (conjugate gradient method). Other authors have used this method [41].

As can be seen in Table 2, the original material had a negligible amount of surface oxygen groups. After the oxidation treatments, the number of surface oxygen groups increased, being the treatment with HNO_3 at boiling temperature during 2 h (NcTb2) the most effective at creating functional groups. In addition, it is observed that the ratio CO/CO_2, which can be taken as a measure of the surface acidity [42], decreased as the severity of the treatment increased.

Deconvolution of CO_2 profiles showed that carboxylic groups were mainly created. It is expected that these groups decrease the hydrophobic character of the carbon materials, improving their interaction with the metal. On the other hand, deconvolution of CO profiles showed that phenols, quinones, and carbonyls were mainly created. It is expected that these groups, which are stable at higher temperatures, act as metal anchoring sites, hindering the agglomeration of metal particles [42].

In order to further investigate how the pore structure and textural properties of the Vulcan XC-72R were changed during the oxidation treatments (see Section 2.1 for oxidation treatments details), supports were characterized by means of N_2-physisorption. Table 3 contains the textural properties of the carbon materials obtained by N_2-physisorption. Vulcan XC-72R has a high specific surface area ($210\,m^2\,g^{-1}$) and a large total pore volume ($0.38\,cm^3\,g^{-1}$). Nevertheless, after the oxidation treatments, the specific surface area of all the samples decreased indicating a partial destruction of the original morphology, being this effect more significant at the carbon material oxidized with the most severe treatment (Vulcan NcTb2). However, no significant change

Table 4: Metal load of the carbon-supported Fe electrocatalysts.

Electrocatalysts	% metal (wt.)
Fe/Vulcan	16.7
Fe/Vulcan NSTa0.5	18.4
Fe/Vulcan NcTb0.5	18.9
Fe/Vulcan NcTb2	21.8

was observed in the pore volume. In fact, carbon supports are mainly mesoporous materials but also contain an appreciable amount of micropores, which is maintained after the surface oxidation. Results suggest that all carbon materials present a broad pore size distribution (PSD) in the range of mesoporosity.

3.2. Physicochemical Characterization of the Electrocatalysts. The catalysts metal loading was determined by SEM-EDX. All catalysts present similar iron content to the nominal value of 20% (Table 4). However, a clear correlation between oxygen groups present in the surface and metal loading can be discerned. As the number of oxygenated groups increased, the amount of deposited Fe increased, since these oxygenated groups acted as anchoring sites. Additionally, homogeneous metal dispersion and deposition on all the carbon materials was observed by SEM images.

Fe/C catalysts were analyzed by XRD technique and their patterns are given in Figure 2. In all the electrocatalysts, except in the sample Fe/Vulcan NSTa0.5, six characteristic peaks appeared at $2\theta = 30.1, 35.5, 43.1, 57.0, 62.6$, which can be assigned to (2 2 0), (3 1 1), (4 0 0), (5 1 1), and (4 4 0) planes of Fe_3O_4 (magnetite) (JCPDS 88-0866), respectively. No diffraction peaks corresponding to iron metal or iron oxides species (FeO or Fe_2O_3) were observed. However, the intensity of the Fe_3O_4 diffraction peaks was not so relevant than that expected for 20 wt.% of iron load. This result suggests that another crystal phase with particle size inferior to 2 nm coexisted with Fe_3O_4 crystals and/or part of the metal was deposited on carbon materials forming a stable but not crystalline structure. In this context, it is important to mention that particle size smaller than 2 nm cannot be achieved by XRD analysis. Other authors have obtained similar results depositing Fe on carbon supports [43]. Additionally, it is noticeable that the diffraction peak at ca. $2\theta = 25°$, which is associated to the graphite (002) diffraction line of the support, is still observed after the iron deposition.

Textural properties of catalysts obtained by N_2-physisorption are summarized in Table 3. Catalysts showed a lower surface area than the corresponding carbon supports, which is attributed to the metal particles loading on the pore surface. In particular, a reduction of the microporosity was observed after the catalysts loading, indicating that the metal was mainly distributed in the micropore structure of the support. PSD continued being broad in the mesoporosity range. However, the pore volume in the 20–50 nm pore diameter range is reduced, whereas in the 50–100 nm pore diameter range is increased. These results indicate that iron

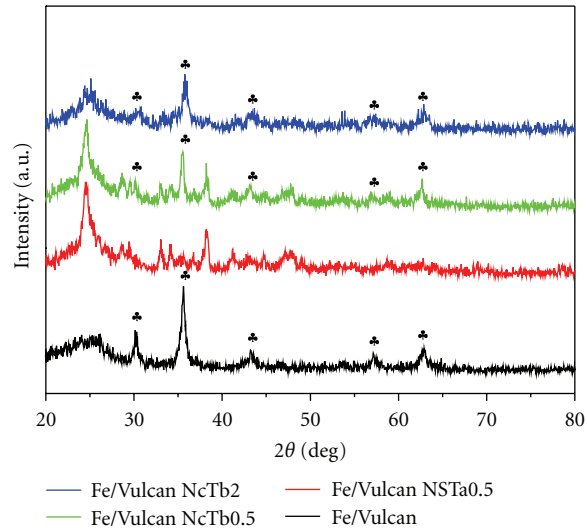

Figure 2: XRD patterns of 20% Fe/C catalysts.

was deposited on the micropores or mesopores with average pore diameter lower than 50 nm, in agreement with the N_2-physisorption results.

3.3. Electrochemical Performances of the Fe Electrocatalysts. The electrochemical properties of the Fe catalysts were studied in 0.5 M H_2SO_4, at room temperature and atmospheric pressure by DEMS. In this sense, DEMS studies provide more information than a simple electrochemical technique (i.e., cyclic voltammetry or chronoamperometry) such as the detection of volatile and gaseous products and intermediates generated in the electrochemical reactions with excellent sensibility. In this context, to the best of our knowledge, this is the first time that CO_2 reduction on carbon-supported Fe catalysts is analyzed by DEMS technique.

First, several potential cycles (not shown) between −0.2 and −1.8 V in 0.5 M H_2SO_4, previously deaerated with Ar, were recorded to clean and activate the catalyst surface. In this context, the voltammetric profile remains similar during the activation step for all catalysts, indicating a minimal (or inexistent) alteration of the electroactive surface. After that, *in situ* spectroelectrochemical experiments were carried out in acid solution with and without dissolved CO_2.

3.3.1. Cyclic Voltammetry (CV) and Mass Spectrometric Cyclic Voltammetry (MSCV). Figure 3 shows the CVs and the corresponding MSCVs for all the carbon-supported Fe catalysts in free CO_2 sulphuric acid solution. The CVs for all the catalysts (Figure 3(a)) present a similar feature, that is, a very high cathodic current at potentials lower than −0.5 V, which may be related to the hydrogen evolution reaction. However, a close inspection of the same figure shows up that the onset potential for the cathodic current starts at different potentials for the different electrodes. The latter becomes clear from the MSCVs for $m/z = 2$ (Figure 3(c)), which is related to the molecular hydrogen formation. Therefore, it is possible to state that the previous carbon treatment

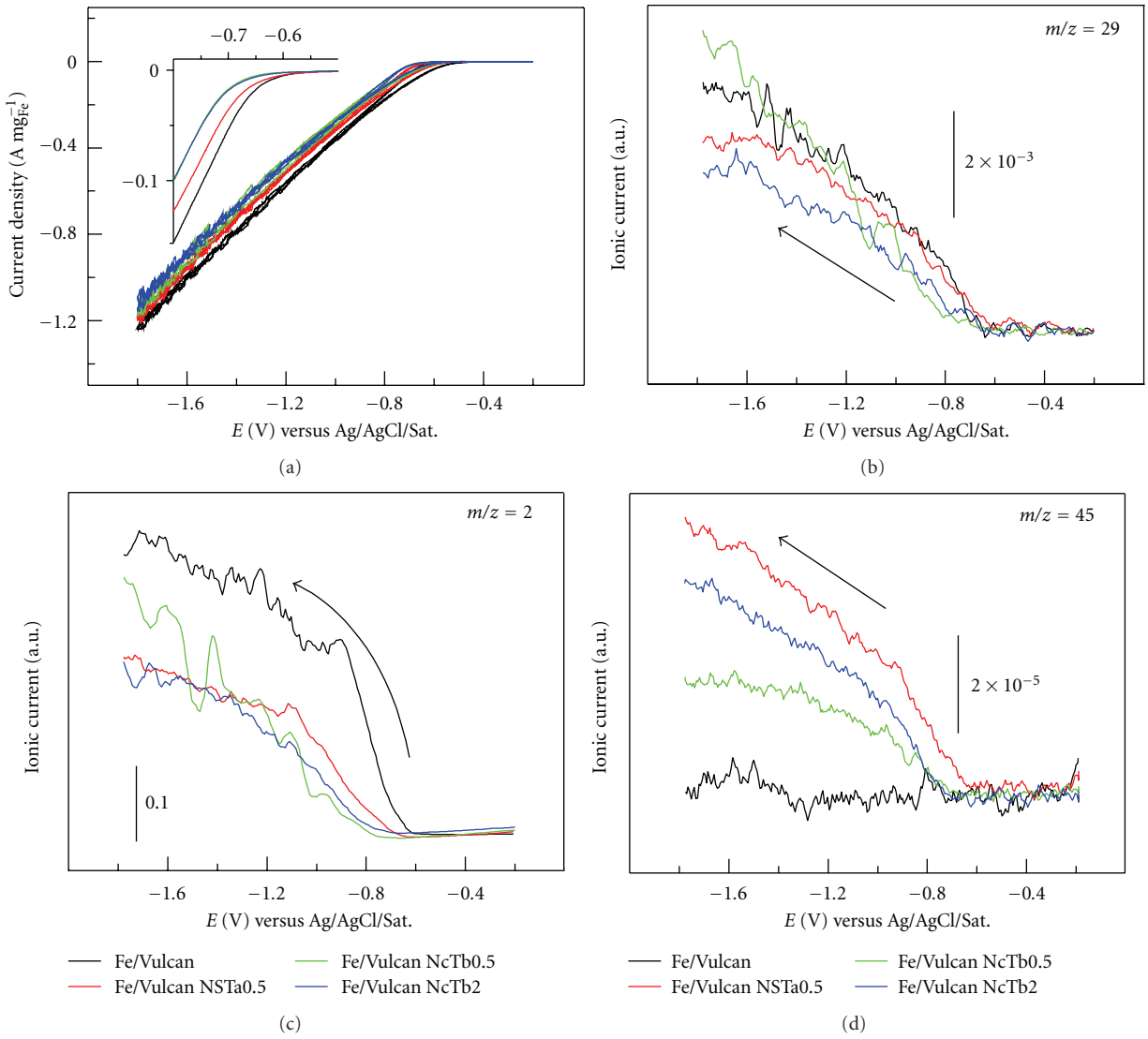

FIGURE 3: CVs and MSCVs for Fe/C catalysts in 0.5 M H_2SO_4 (sweep rate 10 mV s^{-1}, $E_i = -0.2$ V versus Ag/AgCl/Sat.). Inset shows a zoom of the onset potential region during the cathodic scan.

influences the water electro-reduction, and that the catalytic activity towards this reaction on the present Fe/C electrodes in a CO_2 free acid solution increases in the following way: Fe/Vulcan NcTb2 ≈ Fe/Vulcan NcTb0.5 < Fe/Vulcan NSTa0.5 ≪ Fe/Vulcan. Also, it is important to mention that the electrochemical behavior of all the electrodes remains similar after the electrochemical study without CO_2. The latter indicates that the electroactive surface is not damaged (or it is minimum) by these experiments.

Additionally to the H_2 formation, the mass signals m/z = 16 (CH_4^+: methane), 30 ($CH_3CH_3^+$ or H_2CO^+: ethane or formaldehyde), 29 ($CH_3CH_2^+$ or CHO^+: ethane/ethanol or an aldehyde), and 45 ($HCOO^+$ or CH_3CHOH^+: formic acid or ethanol) were monitored during the cathodic scan. Figures 3(b) and 3(d) show the only two signals (m/z = 29 and 45) that increase during the excursion toward negative potentials. In this condition (no presence of dissolved CO_2), the species associated to the mass signals 29 and 45 must be formed from the carbon support degradation. Interestingly, the mass signal 45 depends strongly on the carbon support treatment and its intensity rises in the order: Fe/Vulcan < Fe/Vulcan NcTb0.5 < Fe/Vulcan NcTb2 < Fe/Vulcan NSTa0.5. It is noticeable that the onset potential for the mass signal 45 formation at the catalyst previously treated with a mix of nitric and sulphuric acid is much lower than at the other catalysts (around 0.2 V), while the nontreated catalyst (Fe/Vulcan) presents a very small m/z = 45 signal at potentials more negative than −1.3 V. In the same way, both catalysts treated only with nitric acid develop the same onset potential for this m/z ratio, but its production on the Fe/Vulcan NcTb2 is somehow higher.

On the other hand, the ion current intensity and onset potential for the mass signal 29 are quite similar for all Fe/C catalysts. However, a close inspection of this figure shows

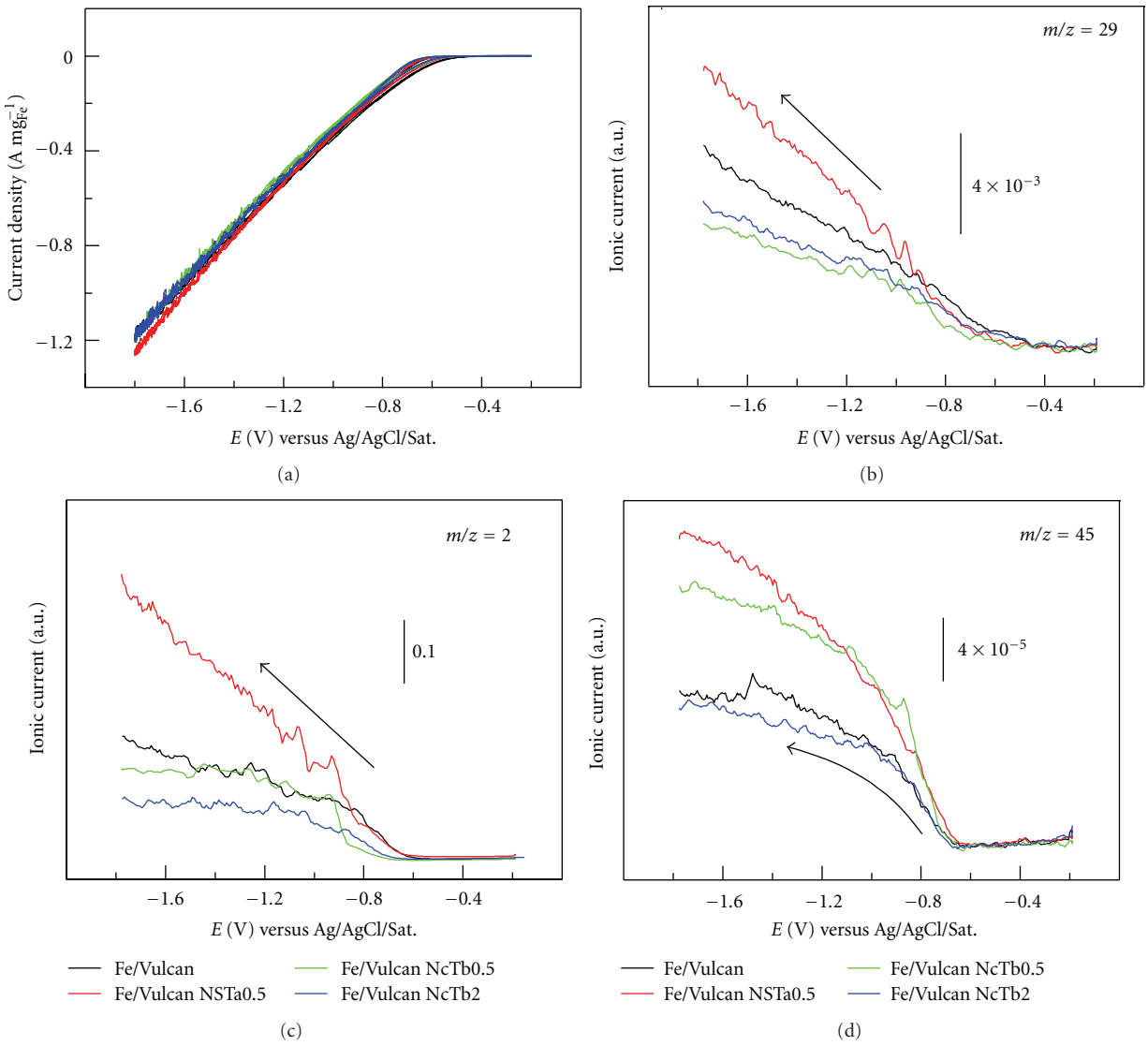

Figure 4: CVs and MSCVs for CO_2-saturated solution in 0.5 M H_2SO_4 on Fe/C catalysts (sweep rate 10 mV s^{-1}, E_i = −0.2 V versus Ag/AgCl/Sat.).

a small but visible trend in its production, which diminishes in the subsequent way: Fe/Vulcan > Fe/Vulcan NSTa0.5 > Fe/Vulcan NcTb2. Fe/Vulcan NcTb0.5 catalyst presents a different behavior toward the mass signal 29 production, in which the onset potential is equal to Fe/Vulcan NcTb2 electrode and the ion current intensity increases linearly as the applied potential becomes more negative.

Summarizing, at the present conditions (CO_2-free solution), nontreated catalyst (Fe/Vulcan) presents the highest and lowest catalytic activity towards hydrogen and mass signal 45 production, respectively. Treated catalysts develop similar behavior toward hydrogen evolution and the ionic current for the m/z = 45 depends strongly on the catalyst surface (see Table 2), that is, the mass signal 45 is enhanced on the catalysts that present oxygen groups on the surface. Additionally, mass signal 29 intensity modestly depends on the previous history of the carbon support.

Figure 4 displays the CVs and MSCVs (m/z = 2, 29, and 45) for all the Fe/C catalysts studied in the present work in acidic solution in the presence of dissolved carbon dioxide. Also, the m/z = 16, 30, and 32 were studied, but do not present an ionic current change during the cathodic scan. It is important to note that the intensity as well as the behavior of the mass signals 2, 29 and 45 are totally different to those observed in Figure 3 (in absence of dissolved CO_2). Interestingly, in presence of dissolved CO_2, the hydrogen evolution (Figure 3(c)) decreases on Fe/Vulcan, Fe/Vulcan NcTb0.5 and Fe/Vulcan NcTb2, while it increases on Fe/Vulcan NSTa0.5. Moreover, the latter catalyst presents an onset potential shift to more positive potentials for hydrogen formation reaction, that is, water reduction is favored on Fe/Vulcan NSTa0.5 in CO_2 containing solution. Also, the the ratio m/z = 29 Figure 3(b) changes abruptly when CO_2 is present in the working solution. The ion

current intensity for this mass signal in a CO_2-containing solution is higher than in a CO_2-free one, and it drops off in the sequence: Fe/Vulcan NSTa0.5 > Fe/Vulcan > Fe/Vulcan NcTb2 ≈ Fe/Vulcan NcTa0.5, whereas the onset potential is quite similar for all the electrodes.

On the other hand, Figure 4(d) shows an important enhancement of the mass signal 45 at all the catalysts when CO_2 is present in the solution. These experimental facts unequivocally indicate that carbon dioxide is reduced to form hydrocarbonated compounds such as formic acid. The formation of acids, alcohols, or other molecules, which contain longer hydrocarbon chains, is not discarded but this characterization is not the principal purpose of the present work: the main reasons of the present study are to know if it is possible to electrochemically reduce CO_2 on iron catalysts and to establish if the carbon support influences on this particular reaction. Therefore, only the mass signals 2 and 45 are going to be followed along the present manuscript.

3.3.2. Current Transient (CT) and Mass Spectrometric Transient (MST). Potentiostatic pulse experiments were performed from a potential where nonfaradaic reactions occur ($E_i = -0.2$ V) to a final potential ($E_f = -1.8$ V) where the CO_2 reduction reaction is controlled by mass diffusion. Current transients for all the Fe/C catalysts used in the present work in absence (a) and presence (b) of dissolved CO_2 in sulphuric acid solution can be seen in Figure 5. It is observed similar faradaic current intensities than those obtained during the potentiodymanic experiments (Figures 3(a) and 4(a)), that is, Fe/Vulcan NcTb2 presents at both mediums (in presence and absence of dissolved CO_2) the lowest faradaic current, while the other catalysts develop similar faradaic currents. Consistent with the results presented above, molecular hydrogen production is significantly influenced by the presence of CO_2 (Figure 6). Fe/Vulcan and Fe/Vulcan NSTa0.5 electrodes present the highest catalytic activity toward H_2 formation in absence and presence of CO_2, respectively. Also, it is noticeable that the signal for $m/z = 2$ decreases abruptly on Fe/Vulcan, Fe/Vulcan NcTb0.5, and Fe/Vulcan NcTb2 catalysts, while the same reaction is enhanced on the Fe/Vulcan NSTa0.5 when CO_2 is present in solution.

Figure 7(a) shows the MSTs for the mass signal 45. Currents obtained are of the same order of magnitude than in the voltammetric experiments. However, a close inspection of the curves reveals that the $m/z = 45$ signal continuously increases on Fe/Vulcan catalyst along the time, while the other catalysts present a constant ionic current. The latter suggests that the support time degradation is more important at this material. In this sense, it is important to remind that Fe/Vulcan electrode presents small quantity of oxygenated species on the surface (see Table 2), that is, this catalyst suffers a dreadful condition at this potential. On the other hand, when CO_2 is present in solution (Figure 7(b)) the intensity of the mass signal 45 changes dramatically (about five fold times), as it was observed before the MSCV experiments (Section 3.3.1). In fact, the ionic current intensities for the mass signal 45 grow up on the studied

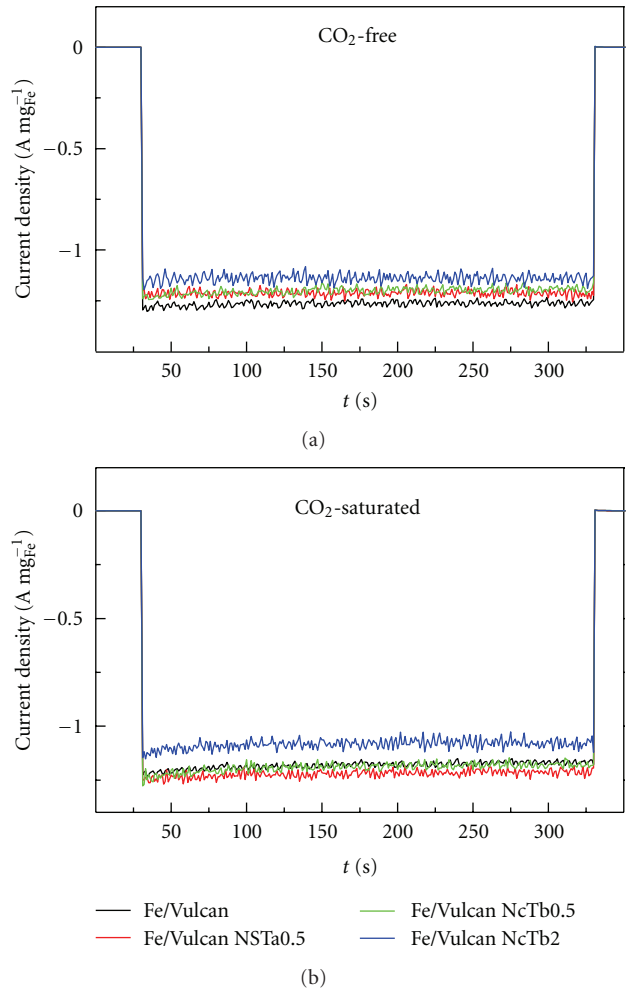

Figure 5: CTs for CO_2-free (a) and CO_2-saturated (b) solution in 0.5 M H_2SO_4 on Fe/C catalysts ($E_i = -0.2$ V, $E_f = -1.8$ versus Ag/AgCl/Sat.).

catalysts in the following way: Fe/Vulcan NcTb2 < Fe/Vulcan < Fe/Vulcan NcTb0.5 < Fe/Vulcan NSTa0.5.

In order to acquire a realistic result of hydrocarbon production from carbon dioxide reduction, the mass signal 45 was subtracted from the ionic current signals obtained with dissolved CO_2 in solution (Figure 7(b)) and those acquired in a CO_2-free solution (Figure 7(a)) and represented in Figure 8. In this context, it is really important to know that this subtraction can be only done if all the parameters concerning to the mass spectrometer are constant [44], and because of this, our mass spectrometer setup was build up to make all this parameters accurate [39]. Therefore, Figure 8 shows a realistic catalytic activity toward carbon dioxide reduction. In fact, it can be observed that the typical features of a reaction controlled by mass diffusion, and even more important that the carbon dioxide reduction, or what is the same in this event, the hydrocarbon production depends strongly on the catalyst support and it increases as follows: Fe/Vulcan NcTb2 < Fe/Vulcan < Fe/Vulcan NSTa0.5 ≈ Fe/Vulcan NcTb0.5.

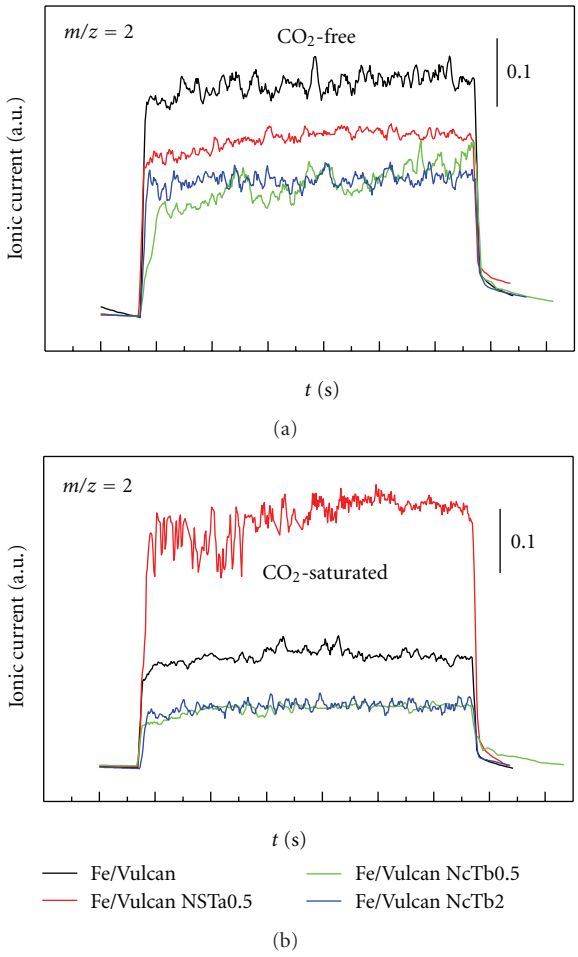

FIGURE 6: MSTs for CO_2-free (a) and CO_2-saturated (b) solution in 0.5 M H_2SO_4 on Fe/C catalysts ($E_i = -0.2$ V, $E_f = -1.8$ versus Ag/AgCl/Sat.).

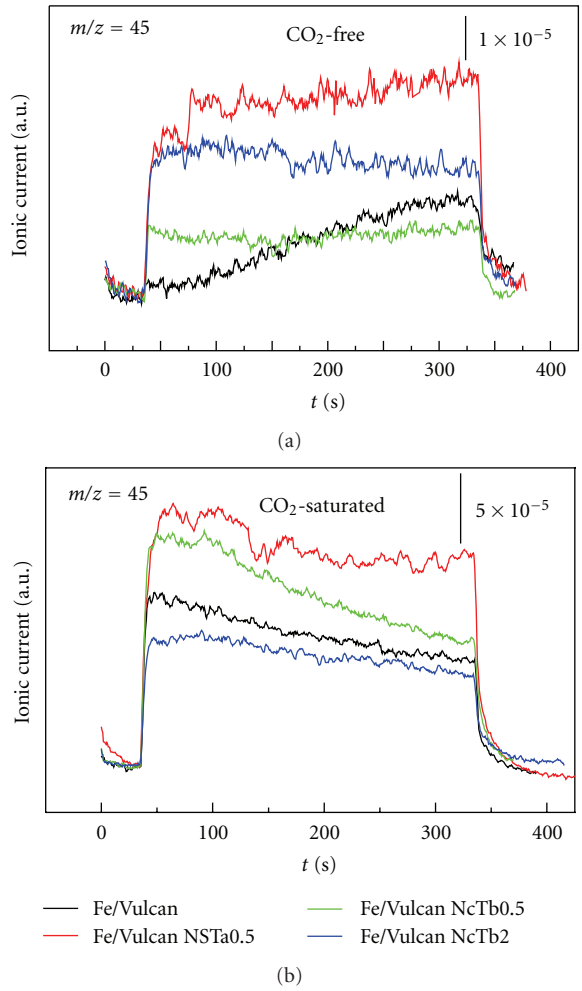

FIGURE 7: MSTs for CO_2-free (a) and CO_2 saturated (b) solution in 0.5 M H_2SO_4 on Fe/C catalysts ($E_i = -0.2$ V, $E_f = -1.8$ versus Ag/AgCl/Sat.).

4. Discussion

Although the electrochemical reduction of carbon dioxide has been hugely studied, the reaction mechanism is not exactly known. Most of the reactions on different metal catalysts at diverse conditions, involving homogeneous and heterogeneous catalysis, were proposed by Sullivan [8] and assume a high availability of protons. In general, four principal pathways can be considered during the carbon dioxide reduction in acidic media [44]: (i) CO(g) formation via disproportionation; (ii) $CO_2^{\bullet -}$ radical formation; (iii) $\bullet COOH_{(ad)}$ formation; (iv) the formation of adsorbed reduced-CO_2 species giving a range of reduced-CO_2 and products (CO, hydrocarbons and alcohols). The main proposed reactions in the CO_2 reduction mechanism are given as follows:

$$CO_2 + e^- \longrightarrow CO_{2(ad)}^{\bullet -}, \quad (1)$$

$$CO_{2(ad)}^{\bullet -} + H^+ \longrightarrow \bullet COOH_{(ad)}, \quad (2)$$

$$CO_{2(ad)}^{\bullet -} + e^- + 2H^+ \longrightarrow CO_{(ad)} + H_2O. \quad (3)$$

From $CO_{(ad)}$ species, a series of products CH_2CO, CH_3CHO, C_2H_5OH, C_2H_4, C_2H_6, C_3H_7OH, and CH_3OH can be formed [44]. On the other hand, $\bullet COOH_{(ad)}$ species can suffer a nucleophilic attack to form $CO_{(ad)}$ or alternatively may be released as formic acid:

$$\bullet COOH_{(ad)} + e^- \longrightarrow COOH_{(ad)}^- \longrightarrow COOH^-, \quad (4)$$

or via hydrated form:

$$\bullet COOH_{(ad)} + e^- + H_2O \longrightarrow HCOOH. \quad (5)$$

Considering the same equations, a mechanism that represents our present study can be proposed. The following mechanism is quite similar to that described by Dubé and Brisard [45] for CO_2 electroreduction on polycrystalline Cu electrodes in acidic media. First, adsorbed hydrogen is formed during the cathodic sweep by the reaction

$$H^+ + e^- \longrightarrow H_{(ad)}, \quad (6)$$

or by water dissociation:

$$H_2O + e^- \longrightarrow H_{(ad)} + OH^-, \quad (7)$$

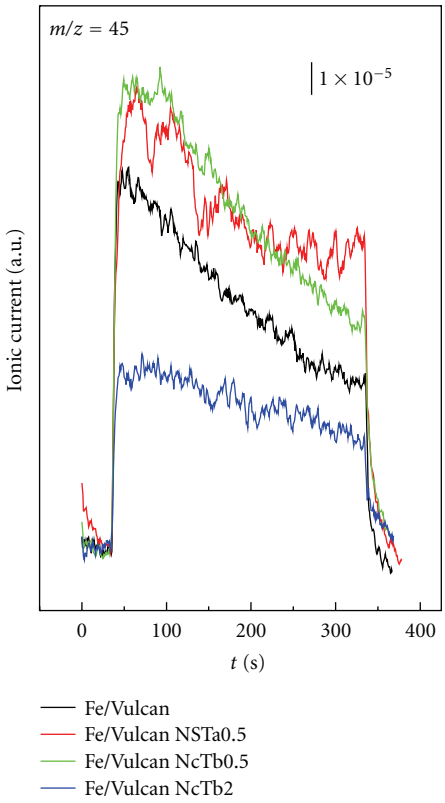

FIGURE 8: Corrected MSTs for CO_2 electroreduction in 0.5 M H_2SO_4 on Fe/C catalysts (E_i = −0.2 V, E_f = −1.8 versus Ag/AgCl/Sat.).

followed by hydrogen evolution:

$$2H_{(ad)} \longrightarrow H_2. \quad (8)$$

Then, carbon dioxide bubbled trough the solution may adsorb and react on the iron-based catalysts in acidic solution in the subsequent way:

$$CO_2 \longleftrightarrow CO_{2(ad)}, \quad (9)$$

$$CO_{2(ad)} + 2H_{(ad)} \longrightarrow CO_{(ad)} + H_2O, \quad (10)$$

$$CO_{2(ad)} + H_{(ad)} \longrightarrow COOH_{(ad)}, \quad (11)$$

$$COOH_{(ad)} + H_{(ad)} \longrightarrow HCOOH, \quad (12)$$

$$COOH_{(ad)} + H_{(ad)} \longrightarrow CO_{(ad)} + H_2O. \quad (13)$$

The present mechanism is limited by the hydrogen (6) and carbon dioxide (9) adsorption reactions, which are necessary steps to form hydrogenated molecules. In fact, the availability of protons and the adsorbed hydrogen coverage on the surface have a strong influence on these reactions. Moreover, the metal surface must interact preferentially with a CO_2 species than with adsorbed hydrogen, otherwise, hydrogen evolution reaction will be predominant at the electrode and carbon dioxide reduction reaction will be hindered.

Accordingly, two main pathways are possible.

(i) $CO_{(ad)}$ formation (reaction (10)): the production of this species is favored when the metal surface is highly covered by adsorbed hydrogen and prefer to react with adsorbed carbon dioxide instead of reacting with each other. Therefore, the hydrogen evolution reaction will be apparently inhibited in this event. It seems that this path is governing on Fe/Vulcan NcTb2, Fe/Vulcan, Fe/Vulcan NcTb0.5 catalysts. In fact, it is clearly observed in the MSCVs and MSTs for m/z = 2 of all catalysts (with the exception of Fe/Vulcan NSTa0.5) in absence and presence of dissolved CO_2 (Figures 3, 4, and 6), in which the mass current signal associated to H_2 production decreases in presence of dissolved carbon dioxide. So, these iron catalysts have a preference to adsorb CO_2 instead of producing molecular hydrogen, and consequently, adsorbed hydrogen reacts with adsorbed carbon dioxide to produce hydrogenated species mainly through reaction (10). As it was described before, from adsorbed carbon monoxide it is possible to form products such as HCOH, CH_2CO, CH_3CHO, C_2H_5OH, C_2H_4, C_2H_6, C_3H_7OH and CH_3OH [45, 46].

(ii) $COOH_{(ad)}$ production (reaction (11)): this pathway gives mainly formic acid as a final product (reaction (12)). Reaction (11) is favoured on surfaces with preference to produce molecular hydrogen, and therefore, with a low H_2 coverage. In other words, adsorbed hydrogen species prefer to react with each other to form molecular hydrogen instead to react with adsorbed carbon dioxide. Therefore, hydrogen evolution reaction is usually favoured in parallel to this reaction. Nevertheless, adsorbed carbon monoxide formation (reaction (13)) cannot be discarded. Thus, if $CO_{(ad)}$ is produced, the operative mechanism will be the same than that described above (reaction path i). In this context, Fe/Vulcan NSTa0.5 catalyst is the only one that does not follow the behavior observed for the other catalysts. In fact, this catalyst enhances the hydrogen evolution (m/z = 2) and mass signal 45 in presence of CO_2. The latter suggests that Fe/Vulcan NSTa0.5 catalyst follows principally the reaction path (ii).

Furthermore, the native oxygenated species on the carbon support may follow the same reactions during the cathodic scan (at least in absence of dissolved CO_2, see Figures 3 and 7(a)).

In this context, the mass signal 29 can be attributed to the first reaction path (i), while m/z = 45 can be associated with formic acid production (ii). Nevertheless, the last mass signal also could be linked to the reaction path (i), that is, it could be related to a fragmentation of a long hydrogenated species such as ethanol, which presents

27, 29, 31, and 45 ion current signals. In this sense, in a forthcoming work, will be discussed in detail the species produced during the carbon dioxide reduction on iron catalysts.

Additionally, it is observed that all the present surface reactions are strongly affected by the carbon support. This statement is observed in the MSCVs for m/z = 2, 29, and 45 in Figures 3 and 4, and strongly confirmed by the MSTs for molecular hydrogen and formic acid production depicted in Figures 6 and 7, respectively. It seems that surface oxygen groups enhance the catalytic activity toward CO_2 reduction. However, Fe/Vulcan NcTb2 presents the lowest ion current intensities, suggesting that longer treatment times of carbon support in nitric acid destroy (at least partially) the support structure, and consequently, the catalytic activity towards CO_2 diminishes.

On the other hand, the surface chemistry of the carbon support could explain the different catalytic activity toward CO_2 reduction recorded on Fe/Vulcan NSTa0.5. Vulcan NSTa0.5 is the only support that suffered the oxidation treatment at ambient temperature in the presence of nitric and sulphuric acid. A temperature effect must be discarded since the material catalyst supported on untreated Vulcan follows the same behavior than the other catalysts. Therefore, the presence of sulphuric acid in the treatment that provides high quantity of oxygenated species on the surface seems to be the main responsible for the different behavior observed during the carbon dioxide reduction on Fe/Vulcan NSTa0.5 electrode.

5. Conclusions

Fe catalysts supported on Vulcan XC-72R were synthesized by the polyol method, using ethylenglycol as solvent and reducing agent. Before the metal deposition, surface chemistry of the Vulcan was modified by different oxidation treatments in order to study the influence of the surface chemistry of the support on the catalytic properties of the materials. During these treatments surface oxygen groups were created, being HNO_3 treatment at boiling temperature for 2 h the most effective in creating functional groups, while HNO_3-H_2SO_4 treatment at room temperature produces the highest CO/CO_2 ratio of functional groups in the surface. These treatments strongly affect the behavior of the iron-based catalysts toward the carbon dioxide reduction. In fact, two main reaction paths were identified during the carbon dioxide reduction, both influenced by the surface properties of the carbon support. Additionally, these treatments also modified the textural and morphological properties of Vulcan. A decrease of the surface area, as well as a partial destruction of its structure, was observed as the severity of oxidation treatments increased. Finally, Fe/Vulcan NSTa0.5 and Fe/Vulcan NcTb0.5 present the highest and lowest catalytic activity toward the hydrogen evolution reaction, though both catalysts develop the highest production of the mass signal 45 (formic acid and/or higher carbon-chain products) in presence of dissolved CO_2.

Acknowledgments

The authors gratefully acknowledge financial support given by MICINN (MAT2008-06631-C03-01 and 02) and Gobierno de Aragón and Obra Social La Caixa (GA-LC-008/2009). S. Pérez-Rodríguez acknowledges Gobierno de Aragón for the DGA grant. G. García acknowledges to the JAE program (CSIC) for financial support.

References

[1] S. Ichikawa, "Chemical conversion of carbon dioxide by catalytic hydrogenation and room temperature photoelectrocatalysis," *Energy Conversion and Management*, vol. 36, no. 6–9, pp. 613–616, 1995.

[2] T. Inui, M. Anpo, K. Izui, S. Yanagida, and T. Yamaguchi, *Advances in Chemical Conversions for Mitigating Carbon Dioxide*, Elsevier Science, Amsterdam, The Netherlands, 1998.

[3] M. M. Halmann, *Greenhouse Gas Carbon Dioxide Mitigation*, Lewis, Washington, DC, USA, 1999.

[4] Ch. Song, A. Gaffney, and K. Fujimoto, *CO_2 Conversion and Utilization*, American Chemical Society, Washington, DC, USA, 2009.

[5] F. R. Keene and B. P. Sullivan, "Mechanisms of the electrochemical reduction of carbon dioxide catalyzed by transition metal complexes," in *Electrochemical and Electrocatalytic Reactions of Carbon Dioxide*, B. P. Sullivan, K. Krist, and H. E. Guard, Eds., Elsevier, Amsterdam, The Netherlands, 1993.

[6] M. Aulice Scibioh and V. R. Vijayaraghavan, "Electrocatalytic reduction of carbon dioxide : its relevance and importance," *Journal of Scientific and Industrial Research*, vol. 57, no. 3, pp. 111–123, 1998.

[7] M. M. Halmann, *Chemical Fixation of Carbon Dioxide: Methods for Recycling CO_2 into Useful Products*, CRC Press, Boca Raton, Fla, USA, 1993.

[8] B. P. Sullivan, *Electrochemical and Electrocatalytic Reduction of Carbon Dioxide*, Elsevier Press, Amsterdam, Netherlands, 1993.

[9] T. Weimer, K. Schaber, M. Specht, and A. Bandi, "Methanol from atmospheric carbon dioxide: a liquid zero emission fuel for the future," *Energy Conversion and Management*, vol. 37, no. 6–8, pp. 1351–1356, 1996.

[10] D. Mignard, M. Sahibzada, J. M. Duthie, and H. W. Whittington, "Methanol synthesis from flue-gas CO_2 and renewable electricity: a feasibility study," *International Journal of Hydrogen Energy*, vol. 28, no. 4, pp. 455–464, 2003.

[11] M. Jitaru, "Electrochemical carbon dioxide reduction—Fundamental and applied topics (review)," *Journal of the University of Chemical Technology and Metallurgy*, vol. 42, no. 4, pp. 333–344, 2007.

[12] M. Gattrell, N. Gupta, and A. Co, "A review of the aqueous electrochemical reduction of CO_2 to hydrocarbons at copper," *Journal of Electroanalytical Chemistry*, vol. 594, no. 1, pp. 1–19, 2006.

[13] I. Taniguchi, "Electrochemical and photoelectrochemical reduction of carbon dioxide," in *Modem Aspects of Electrochemistry*, J. O'M. Bockris, R. E. White, and B. E. Conway, Eds., p. 327, Plenum, New York, NY, USA, 1989.

[14] D. L. DuBois, "Electrochemical reactions of carbon dioxide," in *Encyclopaedia of Electrochemistry*, A. J. Bard and M. Stratmann, Eds., pp. 202–225, Wiley-VCH, Weinheim, Germany, 2006.

[15] Y. Hori, H. Wakebe, T. Tsukamoto, and O. Koga, "Electrocatalytic process of CO selectivity in electrochemical reduction of CO_2 at metal electrodes in aqueous media," *Electrochimica Acta*, vol. 39, no. 11-12, pp. 1833–1839, 1994.

[16] Y. Hori, "CO_2 reduction catalyzed by metal electrodes," in *Handbook of Fuel Cells—Fundamentals, Technology and Applications*, W. Vielstich, H. A. Gasteiger, and A. Lamm, Eds., vol. 2, pp. 720–733, John Wiley & Sons, New York, NY, USA, 2003.

[17] M. Azuma, K. Hashimoto, M. Hiramoto, M. Watanabe, and T. Sakata, "Electrochemical reduction of carbon dioxide on various metal electrodes in low-temperature aqueous $KHCO_3$ media," *Journal of the Electrochemical Society*, vol. 137, no. 6, pp. 1772–1778, 1990.

[18] K. Hara, A. Kudo, and T. Sakata, "Electrochemical reduction of carbon dioxide under high pressure on various electrodes in an aqueous electrolyte," *Journal of Electroanalytical Chemistry*, vol. 391, no. 1-2, pp. 141–147, 1995.

[19] S. Nakagawa, A. Kudo, M. Azuma, and T. Sakata, "Effect of pressure on the electrochemical reduction of CO_2 on Group VIII metal electrodes," *Journal of Electroanalytical Chemistry*, vol. 308, no. 1-2, pp. 339–343, 1991.

[20] K. Hara, A. Kudo, and T. Sakata, "Electrochemical reduction of high pressure carbon dioxide on Fe electrodes at large current density," *Journal of Electroanalytical Chemistry*, vol. 386, no. 1-2, pp. 257–260, 1995.

[21] H. De Jesús-Cardona, C. Del Moral, and C. R. Cabrera, "Voltammetric study of CO_2 reduction at Cu electrodes under different $KHCO_3$ concentrations, temperatures and CO_2 pressures," *Journal of Electroanalytical Chemistry*, vol. 513, no. 1, pp. 45–51, 2001.

[22] S. Kaneco, N. H. Hiei, Y. Xing et al., "High-efficiency electrochemical CO_2-to-methane reduction method using aqueous KHCO3 media at less than 273 K," *Journal of Solid State Electrochemistry*, vol. 7, no. 3, pp. 152–156, 2003.

[23] S. Kaneco, N. H. Hiei, Y. Xing et al., "Electrochemical conversion of carbon dioxide to methane in aqueous NaHCO3 solution at less than 273 K," *Electrochimica Acta*, vol. 48, no. 1, pp. 51–55, 2002.

[24] M. Azuma, K. Hashimoto, M. Hiramoto, M. Watanabe, and T. Sakata, "Carbon dioxide reduction at low temperature on various metal electrodes," *Journal of Electroanalytical Chemistry*, vol. 260, no. 2, pp. 441–445, 1989.

[25] T. Saeki, K. Hashimoto, N. Kimura, K. Omata, and A. Fujishima, "Electrochemical reduction of CO_2 with high current density in a CO_2 + methanol medium at various metal electrodes," *Journal of Electroanalytical Chemistry*, vol. 404, no. 2, pp. 299–302, 1996.

[26] T. Saeki, K. Hashimoto, N. Kimura, K. Omata, and A. Fujishima, "Electrochemical reduction of CO_2 with high current density in a CO_2 + methanol medium II. CO formation promoted by tetrabutylammonium cation," *Journal of Electroanalytical Chemistry*, vol. 390, no. 1-2, pp. 77–82, 1995.

[27] K. Ohta, M. Kawamoto, T. Mizuno, and D. A. Lowy, "Electrochemical reduction of carbon dioxide in methanol at ambient temperature and pressure," *Journal of Applied Electrochemistry*, vol. 28, no. 7, pp. 717–724, 1998.

[28] S. Ohya, S. Kaneco, H. Katsumata, T. Suzuki, and K. Ohta, "Electrochemical reduction of CO_2 in methanol with aid of CuO and Cu_2O," *Catalysis Today*, vol. 148, no. 3-4, pp. 329–334, 2009.

[29] S. Kaneco, K. Iiba, H. Katsumata, T. Suzuki, and K. Ohta, "Electrochemical reduction of high pressure CO_2 at a Cu electrode in cold methanol," *Electrochimica Acta*, vol. 51, no. 23, pp. 4880–4885, 2006.

[30] S. Kaneco, K. Iiba, K. Ohta, and T. Mizuno, "Electrochemical reduction of carbon dioxide on copper in methanol with various potassium supporting electrolytes at low temperature," *Journal of Solid State Electrochemistry*, vol. 3, no. 7-8, pp. 424–428, 1999.

[31] T. Mizuno, A. Naitoh, and K. Ohta, "Electrochemical reduction of CO_2 in methanol at -30°C," *Journal of Electroanalytical Chemistry*, vol. 391, no. 1-2, pp. 199–201, 1995.

[32] P. A. Christensen, A. Hamnett, A. V. G. Muir, and N. A. Freeman, "CO_2 reduction at platinum, gold and glassy carbon electrodes in acetonitrile. An in-situ FTIR study," *Journal of Electroanalytical Chemistry*, vol. 288, no. 1-2, pp. 197–215, 1990.

[33] J. P. Hindermann, G. J. Hutchings, and A. Kiennemann, "Mechanistic aspects of the formation of hydrocarbons and alcohols from CO hydrogenation," *Catalysis Reviews*, vol. 35, no. 1, pp. 1–127, 1993.

[34] K. Hara, A. Kudo, and T. Sakata, "Electrochemical CO_2 reduction on a glassy carbon electrode under high pressure," *Journal of Electroanalytical Chemistry*, vol. 421, no. 1-2, pp. 1–4, 1997.

[35] C. W. B. Bezerra, L. Zhang, H. Liu et al., "A review of heat-treatment effects on activity and stability of PEM fuel cell catalysts for oxygen reduction reaction," *Journal of Power Sources*, vol. 173, no. 2, pp. 891–908, 2007.

[36] Y. Shao, G. Yin, J. Zhang, and Y. Gao, "Comparative investigation of the resistance to electrochemical oxidation of carbon black and carbon nanotubes in aqueous sulfuric acid solution," *Electrochimica Acta*, vol. 51, no. 26, pp. 5853–5857, 2006.

[37] C. Prado-Burguete, A. Linares-Solano, F. Rodríguez-Reinoso, and C. S. M. de Lecea, "The effect of oxygen surface groups of the support on platinum dispersion in Pt/carbon catalysts," *Journal of Catalysis*, vol. 115, no. 1, pp. 98–106, 1989.

[38] M. J. Lázaro, L. Calvillo, V. Celorrio, J. I. Pardo, S. Perathoner, and R. Moliner, "Study and application of carbon black Vulcan XC-72R in polymeric electrolyte fuel cells," in *Carbon Black: Production, Properties and Uses*, I. J. Sanders and T. L. Peeten, Eds., 2011.

[39] S. Pérez Rodríguez, M. Corengia, G. García, F. C. Zinola, M. J. Lázaro, and E. Pastor, "Gas diffusion electrodes for methanol electro-oxidation studied by a new DEMS configuration: Influence of the diffusion layer," accepted for publication in *International Journal of Hydrogen Energy*.

[40] J. L. Figueiredo, M. F. R. Pereira, M. M. A. Freitas, and J. J. M. Órfão, "Modification of the surface chemistry of activated carbons," *Carbon*, vol. 37, no. 9, pp. 1379–1389, 1999.

[41] D. Sebastián, I. Suelves, R. Moliner, and M. J. Lázaro, "The effect of the functionalization of carbon nanofibers on their electronic conductivity," *Carbon*, vol. 48, no. 15, pp. 4421–4431, 2010.

[42] C. Prado-Burguete, A. Linares-Solano, F. Rodríguez-Reinoso, and C. S. M. de Lecea, "The effect of oxygen surface groups of the support on platinum dispersion in Pt/carbon catalysts," *Journal of Catalysis*, vol. 115, no. 1, pp. 98–106, 1989.

[43] X. Liu, R. Tang, Q. He, X. Liao, and B. Shi, "Fe(III)-loaded collagen fiber as a heterogeneous catalyst for the photo-assisted decomposition of malachite green," *Journal of Hazardous Materials*, vol. 174, no. 1–3, pp. 687–693, 2010.

[44] O. Wolter and J. Heitbaum, "Differential electrochemical mass spectroscopy (dems)- a new method for the study of electrode processes," *Physical Chemistry*, vol. 88, no. 1, pp. 2–6, 1984.

[45] P. Dubé and G. M. Brisard, "Influence of adsorption processes on the CO_2 electroreduction: an electrochemical mass spectrometry study," *Journal of Electroanalytical Chemistry*, vol. 582, no. 1-2, pp. 230–240, 2005.

[46] R. P. S. Chaplin and A. A. Wragg, "Effects of process conditions and electrode material on reaction pathways for carbon dioxide electroreduction with particular reference to formate formation," *Journal of Applied Electrochemistry*, vol. 33, no. 12, pp. 1107–1123, 2003.